Heliyon 10 (2024) e33868

Contents lists available at ScienceDirect

Heliyon

journal homepage: www.cell.com/heliyon

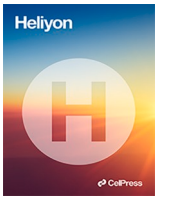

Research article

In vivo evaluation of bioactivity of alginate/chitosan based osteoplastic nanocomposites loaded with inorganic nanoparticles

Oleksii Korenkov, Liudmyla Sukhodub, Mariia Kumeda *, Olha Sukhonos, Leonid Sukhodub

Sumy State University, 116, Kharkivska St., Sumy, 40007, Ukraine

ARTICLE INFO

Keywords:
Osteoplastic nanocomposites
Biopolymers
Hydroxyapatite
Brushite
Femur
Reparative osteogenesis

ABSTRACT

The influence of two nanostructured osteoplastic materials with different compositions: i) alginate (Alg) matrix, loaded with Zn^{2+} ions and nanostructured hydroxyapatite (HA) - S1/HA-Zn, and ii) chitosan (CS) matrix loaded with brushite nanoparticles (NPs, dicalcium phosphate dihydrate, DCPD) - S2/DCPD on the healing of an experimental femoral diaphysis defect was investigated. The structure of cellular elements and the lacunar tubular system of the regenerated bone tissue were studied by electron microscopy. Osteogenic cells on the surface and inside S1/HA-Zn formed bone tissue. On the 30th day, the latter had a reticulofibrous and later lamellar structure. On the 30th day, the S2/DCPD biomaterial was integrated mainly into connective tissue and, starting from the 90th day, into the bone tissue, which was formed only on its outer surface. Thus, it has been proven that both biomaterials contribute to the healing of bone wounds. The regenerative potential of the new bone tissue formation of S1/HA-Zn prevails over that of S2/DCPD.

1. Introduction

To date, autografts and allografts have been traditionally used to optimize the restoration of damaged bone. However, due to the restricted availability of autografts and allografts, the potential for infection, immune incompatibility, bleeding, and functional limitations, scientists are constantly improving the development of biomaterials and tissue-engineered structures [1]. In the last decade, the attention of researchers has been increasingly attracted by biodegradable (bioresorbable) materials, with the main goal of helping the damaged organ regain lost function without the need for repeated reimplantation surgery. One of the main requirements for bioresorption materials is their dissolution in the body without the release of metabolically harmful substances and the formation of a fibrous border. The group of biodegradable materials includes phosphates, calcium sulfates, carbonates, bioglass, as well as the most common calcium hydroxy and fluorapatite [2]. Modern nanocomposite structures are obtained by combining two different systems: a polymer phase and a mechanically strong phase (usually ceramics), which combine the mechanical properties of the inorganic component and the elasticity of polymers. A new trend in biomaterials science is nanoparticle (NP) modification of 3D scaffolds to improve or alter their properties, functionality, and drug release kinetics [3,4]. NPs are characterized by a large specific surface, which gives the material new unique optical, electronic, catalytic, mechanical, and biological properties [5]. The antimicrobial properties of metal NPs (Zn, Cu, etc.) and metal oxides, in particular, ZnO, make them effective antibacterial agents [6].

* Corresponding author. Sumy State University, Kharkivska Str. 2, 40007, Sumy, Ukraine.
E-mail address: mariyakumeda@gmail.com (M. Kumeda).

https://doi.org/10.1016/j.heliyon.2024.e33868
Received 29 March 2024; Received in revised form 27 June 2024; Accepted 28 June 2024
Available online 3 July 2024

It should also be noted that the addition of antibiotics, silver (Ag) or zinc (Zn) nanoparticles to HA helps to eliminate infection and bacterial growth in the implantation site [6–10]. In addition, Zn has a suppressive effect on osteoclast differentiation and increases the viability, adhesion, proliferation, and osteoblast activation of the primary regulatory factors governing osteoblastic differentiation, including the transcription and expression of Wnt-specific genes, at the level of Runx2 and Osterix transcription in bone marrow stromal cell element [11–13].

One of the components of modern biocompatible osteoplastic materials widely used to repair bone defects is the inorganic constituents of bone, hydroxyapatite (HA) or its synthetic analog, as well as biopolymers such as alginate, chitosan, gelatin, and collagen. Nano-HA is a biocompatible, non-toxic, and bioactive material with osteoconductive properties and high absorption activity, which promotes the proliferation and differentiation of osteogenic cells. For the adsorption of proteins during bone regeneration, the group of Dhivya et al. [14] developed a composite material based on zinc-doped CS in combination with nHA and beta-glycerophosphate. These materials have a high level of swelling and stimulate exogenous biomineralization due to nHA. However, it is known that excessive concentrations of nanoparticles can induce oxidative stress as a consequence of the generation of reactive oxygen species (ROS) [15]. Also, HA is a fragile material characterized by a low biodegradation rate [16,17]. In turn, natural polymers are also biocompatible and non-toxic materials and have low mechanical strength and a relatively high biodegradation rate [18,19]. HA and natural polymers in a single biocomposite material combine the advantages of individual components and offset their disadvantages by improving mechanical properties [20]. In addition, biocomposite materials can regulate the resorption rate by increasing or decreasing the percentage of its components [21]. The combination of natural polymers chitosan (CS) and alginate (Alg) in one implant significantly improves its mechanical and biological properties. Osteoblasts on such a chitosan-alginate scaffold are well suited for adhesion, proliferation, and the formation of a mineralized bone matrix [22].

The scientific literature presents studies in which hydroxyapatite is combined with vitamin D to improve its regenerative properties. In this case, osteoblast precursors can convert the inactive form of vitamin D (cholecalciferol) into the active form (1.25 $(OH)_2D3$), which promotes the differentiation of stem cells into mature osteoblasts, increases the expression of osteoblast markers (osteocalcin, alkaline phosphatase), osteocytes (dentin matrix protein-1 and fibroblast growth factor-23) and is involved in the mineralization of the extracellular bone matrix [23,24].

This study aims to evaluate the effect of CS- and Alg-based scaffolds loaded with inorganic nanoparticles on the healing of an experimental defect of the long skeleton bone using microscopic and histological examination. To investigate the electron microscopic structure of cellular elements and the lacunar tubular system of regenerated bone tissue formed in the areas of implantation of experimental materials. To our knowledge, there is very little similar data in the scientific literature.

2. Materials and methods

2.1. Alg-HA-Zn nanocomposite

The initial step in the synthesis of hydroxyapatite hydrogel involved the formation of a precipitate during mixing of 0.3 M diammonium hydrogen phosphate $(NH_4)_2HPO_4$ solution (China production) and 0.5 M calcium nitrate $Ca(NO_3)_2{\cdot}4H_2O$ solution (China production), under conditions of a pH value of 10.5 (25 % aqueous solution of ammonia NH_4OH added, China). The obtained suspension was treated in a microwave (MW) oven Samsung M1712NR for 20 min at the power of microwave irradiation is equal 600 W. After washing HA hydrogel was obtained (85 w% moisture) [25].

The resulting hydrogel was thoroughly mixed with the sodium alginate solution (Alg, E401, Mm15.0 kDa, China). The proportion of each component is as follows: HA:Alg = 3:1. The resulting slurry was dropped into 0.25 M $CaCl_2$ (China production), where the beads formed for 18 h. The 0.4 g of obtained beads were cross-linked in a solution of chitosan with vitamin D_2 (24 h), washed, and subsequently cross-linked in a zinc sulfate $ZnSO_4$ x $7H_2O$ solution (China production) for 1 h. Following this, the material was subjected to a washing and drying process at 37 °C. The sample was named S1/HA-Zn.

CS-DCPD nanocomposite was prepared in accordance with the previously described methodology [26]. Briefly, 0.5 M calcium acetate (pH 6.86) and 6 % CS (Mm 150 kDa, Acros organics, USA) in 1 % acetic acid were mixed. The suspension was shaken for 3 h (37 °C, 110 rpm), then dripped into 0.3 M sodium dihydrogen orthophosphate NaH_2PO_4 (pH = 8.0), forming amorphous calcium phosphate (ACP)/CS beads for 24 h. To transform ACP into DCPD (brushite), the beads were microwave-heated at 300 W for 75 s, with each 15-s interval repeated five times. Obtained beads were immersed in 1 % Sodium tripolyphosphate (TPP) $Na_5P_3O_{10}$ with vitamin D_2 (24 h), then washed and dried at 37 °C. The sample was named S2/DCPD.

The *degree of swelling* (SW) [27] was determined by measuring the weight of the samples prior to and after their immersion in phosphate-buffered saline (PBS) (pH 7.2). The beads' *porosity* (P) was determined using the previously published method [28]. The *mechanical properties* were quantified using the original automated equipment. Samples with a diameter of 5 mm and a thickness of approximately 2.0 mm were prepared by cold pressing. The samples were compressed to approximately 12 MPa for a period of 2 min to determine their elastic characteristics, specifically Young's modulus, and compressive strength [29].

The composite *surface morphology was investigated* using a scanning electron microscope (SEM, FEI Inspect S 50). To study the microscopic structure of the regenerated bone tissue cellular elements, the bone with the implant was freed from soft tissues and placed in glutaraldehyde fixative in PBS (pH 7.4) at 4 °C. After 24 h, the samples were washed in PBS and fixed in a 1 % OsO_4 solution (Osmium Tetroxide, 99.95 %, available from Polysciences, Inc.) in phosphate buffer, followed by dehydration in ethanol of increasing concentration (from 70^o to 100^o) and in anhydrous acetone. The samples were glued to the slides with conductive glue. To study the lacunar tubular system of the formed bone tissue of the regenerate, bone fragments with implanted materials without prior fixation were immersed in a 5 % sodium hypochlorite NaClO solution for 30 min, then washed in distilled water, dehydrated in alcohols of

increasing concentration, encased in methyl methacrylate and placed in a vacuum chamber until air to remove air bubbles. The polymerization was carried out in glass bungs for 1 h at 50 °C and then for 1 day at 37 °C. The resulting blocks were cut into 1 mm thick plates with a diamond cutter. A 5 % sodium hypochlorite solution removed the organic matrix from the plates. Demineralization was done using hydrochloric acid, degreased in ether, and dried in air. All the samples were silver plated in a standard vacuum unit of the VUP-5 type and examined using a microscope SEO−SEM Inspect S50–B [30].

2.2. Light microscopy method

Femoral fragments with implanted biomaterials were fixed in a 10 % formalin solution, and demineralization was performed in a 5 % aqueous solution of Trilon B (ethylenediaminetetraacetic acid). Next, the bone samples were processed through an ascending series of alcohols, followed by the preparation of paraffin blocks. Serial sections (5 μm thick) were prepared using a Shandon Finesse 325 sledge microtome (Thermo Scientific, USA). The histological sections of the fragments, stained with hematoxylin and eosin, were analyzed in a light microscope, the Primo Star (Carl Zeiss, Germany), and photographed using a digital camera, the AxioCam ERc 5s (Carl Zeiss, Germany), with digital image output, the ZEN 2 (blue edition) (Carl Zeiss, Germany). At the same time, connective tissue, reticulofibrous, and lamellar bone tissue and the nature of their interaction with the studied biomaterials were determined in the area of rat femur injury.

2.3. In vivo in rat model study

The experimental study was conducted on 36 mature 6-month-old male Wistar rats (200 ± 10 g) in accordance with the rules set forth in the “European Convention for the Protection of Vertebrate Animals Used for Experimental and Other Scientific Purposes”. Following an external examination and subsequent rejection of the rats, which exhibited deviations from the typical norms of motor activity and wool coat condition, the experiment was initiated. Two distinct scaffolds were implanted: one based on an alginate matrix doped with hydroxyapatite (HA) particles and zinc ions (S1/HA-Zn) and another based on a chitosan matrix doped with brushite (DCPD) nanoparticles (S2/DCPD). The procedure was conducted under intramuscular ketamine anaesthesia at a dosage of 50 mg/kg. The mid-thigh area was treated with a 3 % iodine solution. The skin and fascia were incised along their length with a scalpel, the

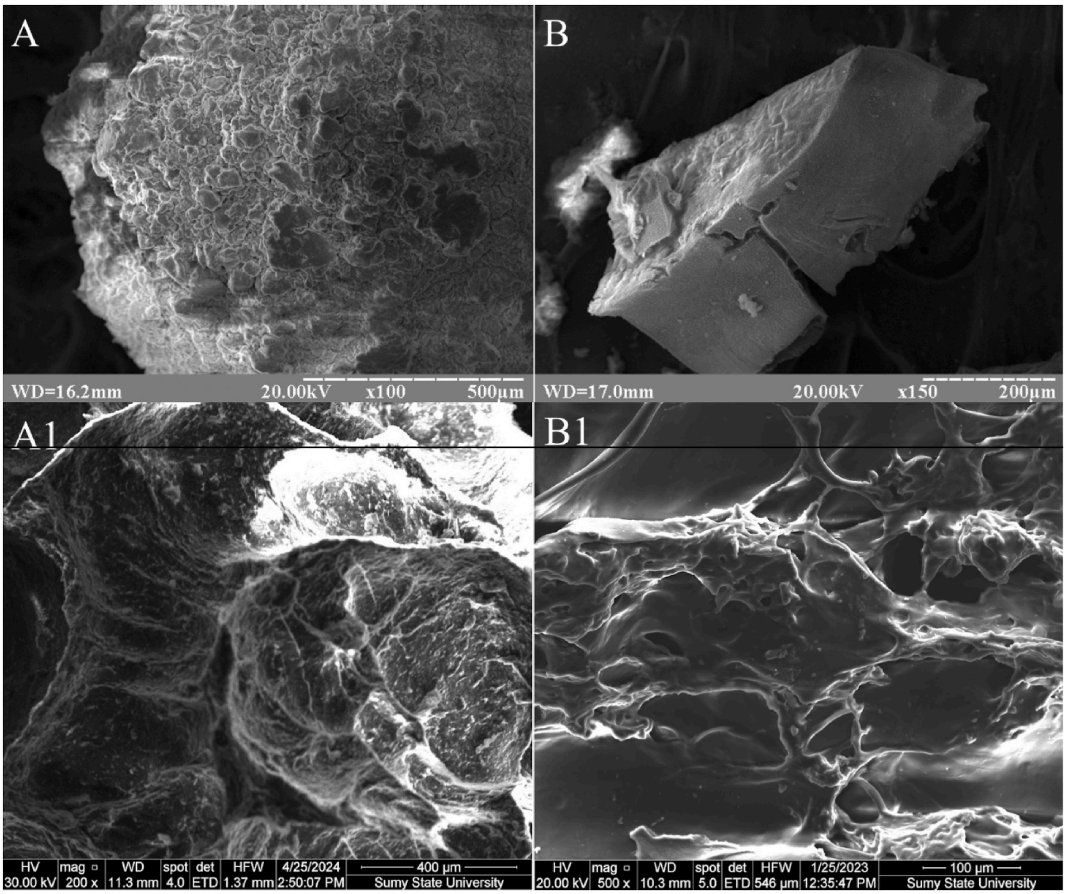

Fig. 1. Light (A, B) and SEM (A1, B1) images of S1/HA-Zn and S2/DCPD, respectively.

muscles were displaced, and the midpoint of the femur's diaphysis was exposed. A defect (diameter D = 2 mm) was created using a ball-shaped dental bur and a dental drill under jet cooling with physiological solution (or 0.9 % sodium chloride solution, to avoid thermal injury to the edges of the defect).

The procedure was successfully concluded with the use of silk sutures for wound closure. Given the nature of the injury, a complete bone fracture was not sustained, thereby obviating the need for additional fixation. All animals were administered subcutaneous buprenorphine at a dose of 0.3 mg/kg of body weight for a period of two days, with an interval of 12 h between doses. The rats were provided with appropriate care, housed on a standard diet, and had unrestricted access to drinking water. The healing of the femoral bone defect under conditions of implantation of scaffolds was examined using light and scanning electron microscopy subsequently, at designated time intervals.

3. Results

In this study, we investigated by light and electron microscopy the *in vivo* behavior of two osteoplastic materials with opposite compositions, namely S1/HA-Zn (Fig. 1 A, A1) based on an Alg matrix and S2/DCPD (Fig. 1 B, B1) based on a CS matrix. It is known that CS is a natural cationite, and Alg is a natural anionite in terms of electrostatic characteristics, which affects the properties of the composite as a whole. Comparative characteristics of both osteoplastic materials (Table 1) are presented in detail in our recent work, which highlights their regenerative potential based on computed tomography (CT) data [31]. Briefly, XRD data show that the annealed at 400 °C in order to increase peak resolution sample S1/HA/Zn contains inorganic phase HA (JCPDS 09–432). Several calcium phosphate (CaP) phases were observed in the S2/DCPD, which were formed during heating at 400 °C. Based on the phase transformations during temperature treatment [31], we conclude about the presence of nanosized DCPD in the composite dried at 37 °C. It is important to note that the identification of DCPD by the XRD method in the composite dried at 37 °C is impossible since the nanosized CaP particles are clusters and do not have a crystalline structure.

By EDX data, the experimental samples contain about 70 % HA (Ca/P = 1.6) and about 25 % DCPD (Ca/P = 1.0), respectively, and demonstrate a relatively low degree of swelling (about 70 %), which is important for osteoplastic materials. The samples have low porosity values (24 % and 11 %, respectively), but new tissue sprouting and vascularization can additionally occur in the space between the beads. The presence of Zn ions in S1/HA-Zn contributes to the porosity and gives the material antimicrobial properties. The component composition affects the mechanical properties; namely, Young's modulus for S2/DCPD is 780 MPa, while for HA/Zn, it is 530 MPa. On the other hand, the compressive strength for S2/DCPD is σ_c = 40 MPa, while for HA/Zn, it is about 270 MPa [29].

It was proved that the formation and maturation of bone tissue regenerate occurred on the surface of both scaffolds (S1/HA-Zn, S2/DCPD), and in the case of S1/HA-Zn, also in its volume. According to the results of CT [31], the optical density (OD) in the S1/HA-Zn and S2/DCPD implantation sites gradually increased to the OD values of native bone during the experiment (Fig. 2 A, B). At the same time, the location of biomaterials not only at the level of the intermedial part of the defect but also in the bone marrow canal led to the appearance of radiological signs of endosteal bone callus, which was traced on a CT scan. The identification of an endosteal bone callus enabled the determination of the location of the initial trauma, despite the absolute OD of the defect area being equivalent to that of the mother bone. Notably, the optical density of the femur of the control group animals, whose defect healed under the blood clot, did not recover in 140 days. Thus, it was proved that both materials are characterized by the ability to optimize reparative osteogenesis successfully. The CT indicates that both biomaterials facilitate the complete 140-day healing of the experimental femoral defect.

In vivo in rat model study. On the 30th day, in the Control animal group, the defect area was filled with bone trabeculae of reticulofibrous bone tissue, which formed small- and large-looped mesh structures. Fibrous connective tissue was located in the intertrabecular space. In the animals of the second and third groups, a significant area of the defect was occupied by S1/HA-Zn and S2/DCPD biomaterials, and the area of their implantation contained bone and connective tissue of the regenerate. In the gap between the bone tissue and S2/DCPD, there was a multicellular fibrous connective tissue in close contact with the biomaterial. At the same time, S2/DCPD underwent fragmentation into small particles, some of which were completely integrated into the connective tissue. In the second animal group, on the surface of the S1/HA-Zn scaffold, osteogenic cellular elements formed regenerate bone tissue, which was tightly adjacent to the cortical layer of the native bone (Fig. 3).

The formed bone tissue had a reticulofibrous or lamellar structure, and osteoblasts and osteocytes were found in its composition (Fig. 4).

Visually, no cartilage tissue was detected in any group of experimental animals, and the amount of connective tissue present in the defect was greater in the Control and S2/DCPD implantation groups, and the least one in animals with implanted S1/HA-Zn. On the 90th day, animals of all groups underwent a reorganization of tissue-specific structures of the regeneration and remodeling of reticulofibrous bone tissue into lamellar bone tissue. However, these processes were still incomplete, since small remnants of

Table 1
The main physical and structural parameters of experimental composites [31].

Parameter	Sw, %	Porosity, %	The content of the inorganic part, %	Mechanical characteristics	
Sample				σ_c, MPa	E, MPa
S2/DCPD	68 ± 0.98	11.04 ± 0.12	23.7 ± 0.95	40	780
S1/HA-Zn	70.5 ± 0.36	24.3 ± 0.22	68.9 ± 0.85	269	526

Note: $p \leq 0.05$.

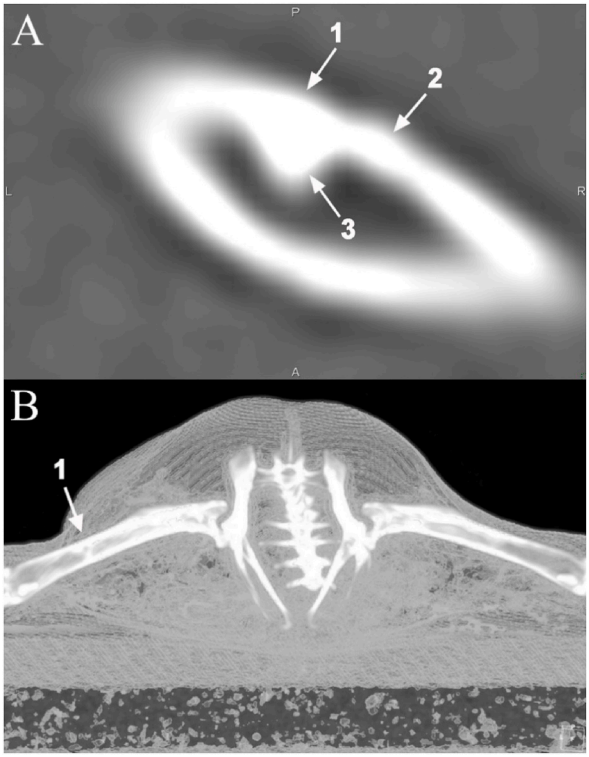

Fig. 2. **A**: CT of the rat femoral diaphysis. The area of the defect on the 140th day after implantation of S1/HA-Zn into its cavity (1). The adjacent native bone to the biomaterial implantation site (2). Endosteal bone callus (3). **B**: 3D model of a CT of the rat femoral diaphysis. The area of the defect on the 140th day after implantation of S2/DCPD (1).

connective and reticular fibrous bone tissue remained around the previous injury in control animals and animals of the third group. At the same time, visually, the area of reticulofibrous bone tissue in the area of injury in animals of all groups significantly decreased compared to day 30 of observation and was replaced by lamellar bone tissue. In animals of the control group, the space between the bone trabeculae was filled with connective tissue and, in some places, bone marrow. The S2/DCPD and S1/HA-Zn biomaterials were in close contact mainly with lamellar bone and, to a lesser extent, with reticular fibrous bone. The S2/DCPD implant underwent partial resorption. The connective tissue between the biomaterials and the regenerate bone tissue was no longer detected at this time of the experiment (Fig. 5).

The regenerated bone tissue contained osteocytes located in bone lacunae, and osteoblasts were located on the surface of bone trabeculae (Fig. 6). In addition, single multinucleated osteoclasts could be observed in the bone tissue, which formed resorption lacunae.

On the 140th day, the defect area was filled with lamellar bone tissue with S2/DCPD and S1/HA-Zn integrated into its structure. The S1/HA-Zn biomaterial occupied a significant area of the previous injury, did not undergo fragmentation, and remained in its original geometric shape. No visible biodegradation of S1/HA-Zn was observed. The outer surface of this composite was covered by a layer of lamellar regenerated bone tissue, which was in close contact with the native bone adjacent to the implantation site. It should be noted that the formation of new bone tissue occurred not only on the outside but also in the middle of S1/HA-Zn, where islands of bone tissue with osteocytes were detected. In the animals of the third group, bone tissue was formed on the outer surface of S2/DCPD and in close contact with the native bone bordering on the implantation site. Osteoblasts and osteocytes were found in the bone tissue of the regenerate.

Osteocyte bodies were located in bone lacunae, and their long processes in bone tubules. Also, multinucleated osteoclasts were found on the surface of the regenerated bone tissue, which ensured its resorption (Figs. 7 and 8).

4. Discussion

Microscopic examination showed that no signs of inflammatory reaction were observed in the S2/DCPD and S1/HA-Zn sites throughout the experiment. On day 30, the S2/DCPD biomaterial underwent fragmentation, and its particles were integrated into the connective tissue of the regenerate. Bone tissue was also formed in the S2/DCPD area, but connective tissue was located between it and the biomaterial. At the same time, S1/HA-Zn did not undergo fragmentation, bone tissue was formed mainly on its outer surface, and no connective tissue layers between the implant and regenerated bone were observed. It should also be noted that in the animals of all experimental groups, the regenerated bone tissue had a predominantly reticulofibrous and, to a lesser extent, lamellar structure.

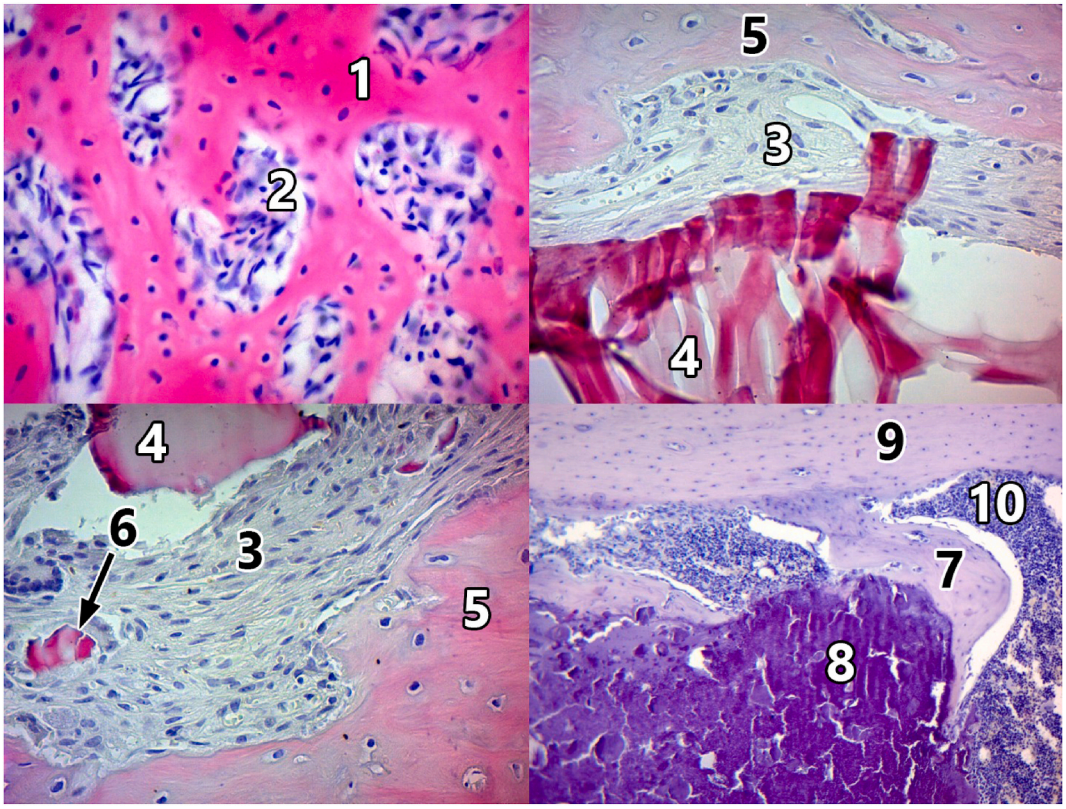

Fig. 3. The rat femoral defect area on day 30 after implantation. Reticulofibrous bone tissue (1) and connective tissue (2) of the regenerate in the Control group (magnification 400). The connective tissue layer (3) between S2/DCPD (4) and regenerated bone tissue (5), integration of a small fragment of S2/DCPD (6) into the connective tissue (3), magnification 400. Formation of regenerated bone tissue (7) directly on the outer surface of S1/HA-Zn (8). The adjacent mother bone to the S1/HA-Zn implantation site (9). Bone marrow (10), magnification 100. Hematoxylin and eosin staining.

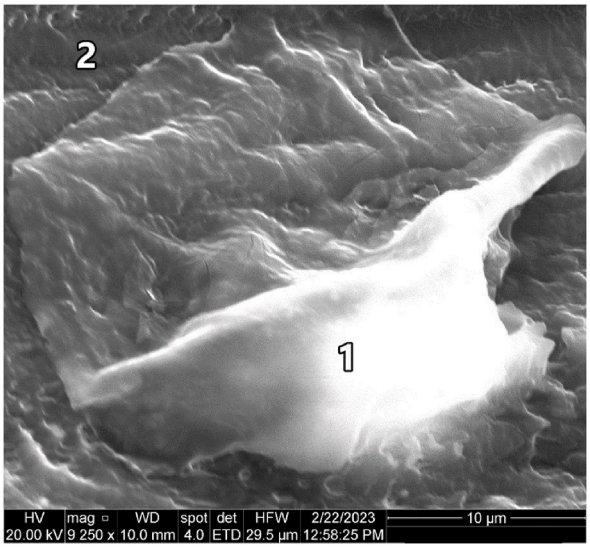

Fig. 4. Osteoblast (1) on the surface of the trabecular reticulofibrous bone tissue of the regenerate (2) in Control group animals on day 30 after the defect. Electronic scan, magnification 9250.

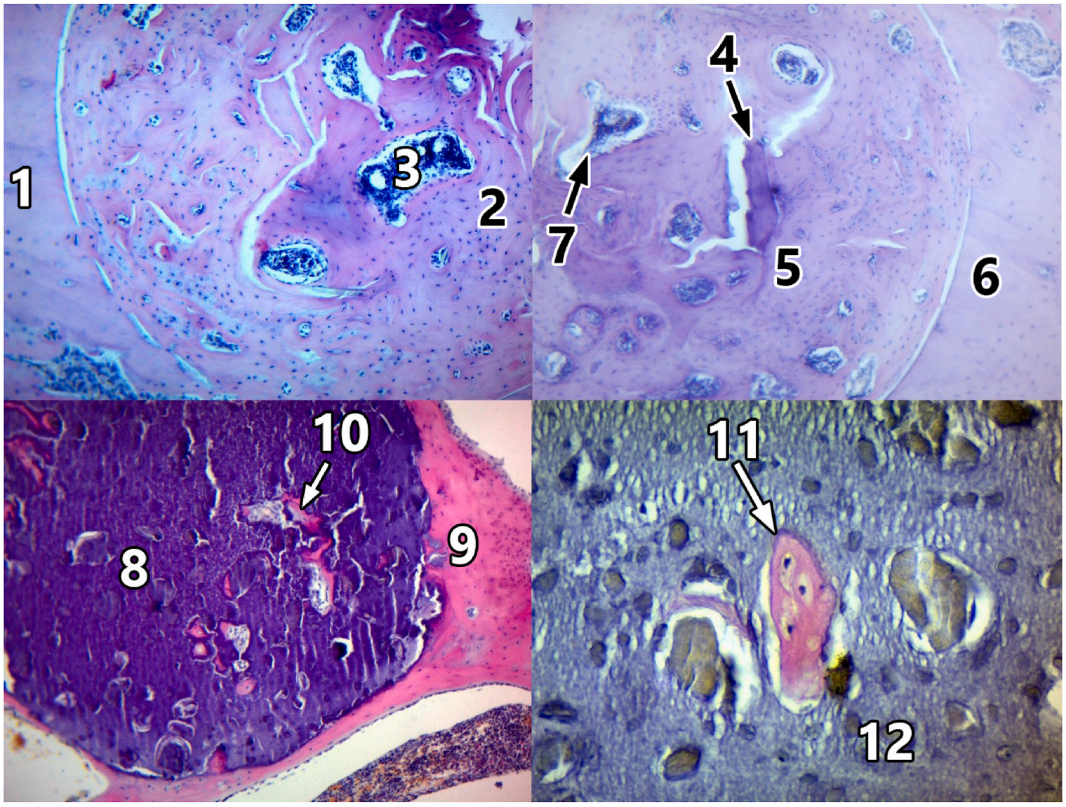

Fig. 5. The area of the rat femoral defect on the 90th day of implantation. Mother bone (1), lamellar bone tissue (2) and connective tissue remnants (3) of the regenerate in the control group. A small fragment of S2/DCPD (4) is integrated into the regenerated bone tissue (5), which is tightly adjacent to the mother bone (6). Remnants of connective tissue (7). Magn. 100. S1/HA-Zn (8) is integrated into the regenerated bone tissue (9). Bone formation (10) in the middle of S1/HA-Zn. Formed bone tissue with osteocytes (11) in the middle of S1/HA-Zn (12). Magn. 400. Hematoxylin and eosin staining.

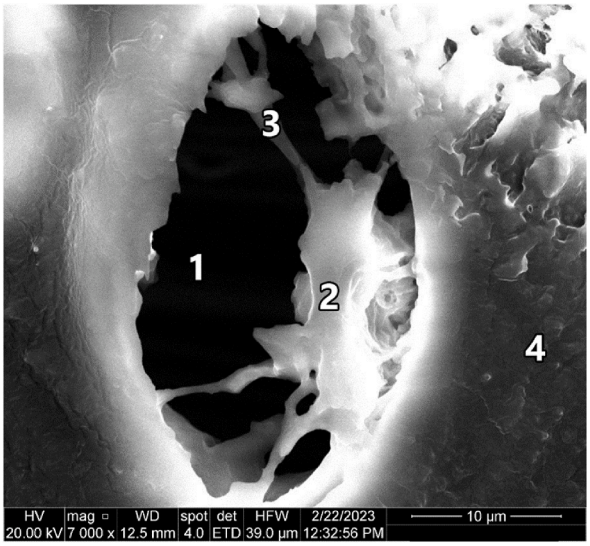

Fig. 6. Bone lacuna (1), body (2), and processes (3) of an osteocyte in the regenerated bone tissue (4), which formed in the middle of the S1/HA-Zn biomaterial on the 90th day after implantation. Electronic scan, magnification 7000.

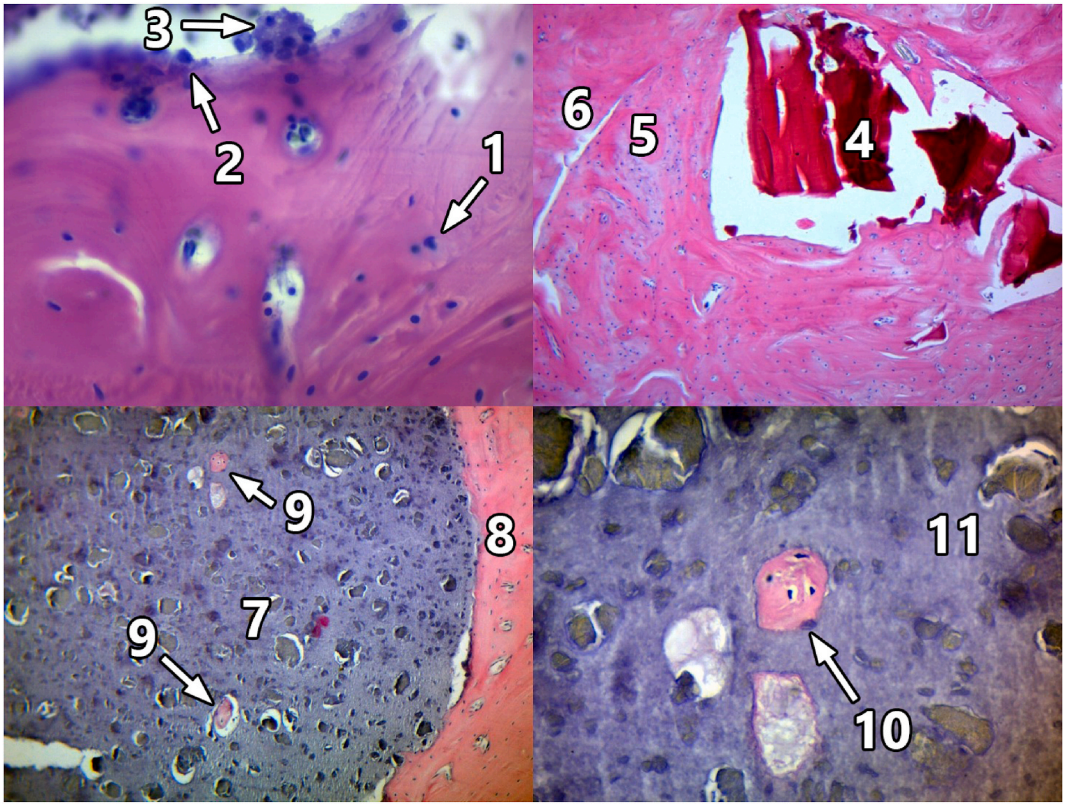

Fig. 7. The area of the rat femur defect on day 140 after implantation. Osteocyte (1), osteoblast (2), and osteoclast (3) in the bone tissue of the regenerate of the control group, magnification 400. Fragments of S2/DCPD (4) are integrated into the lamellar bone tissue of the regenerate (5), which is tightly adjacent to the mother bone (6), magnification 100. S1/HA-Zn (7) is integrated into the regenerated bone tissue (8). Bone formation (9) in the middle of S1/HA-Zn, magnification 100. Formed bone tissue with osteocytes (10) in the middle of S1/HA-Zn (11), magnification 400. Hematoxylin and eosin staining.

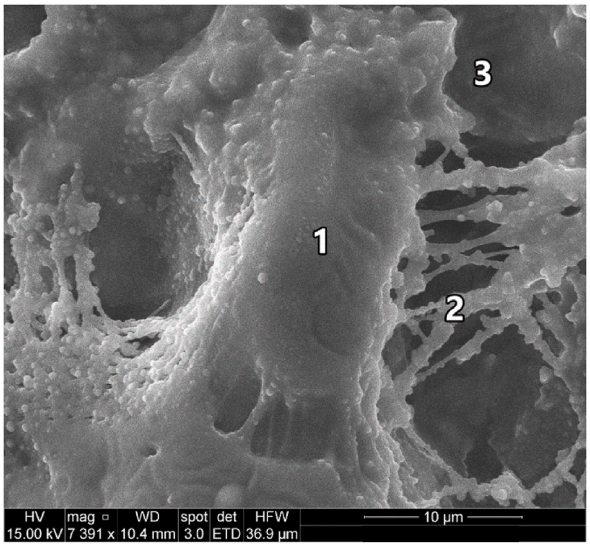

Fig. 8. Polymeric replica of a cellular bone lacuna (1) with tubules (2) in the regenerated bone tissue (3), which was formed on the surface of S2/DCPD biomaterial on the 140th of implantation. Microcorrosion preparation. Electronic scan, magnification X7391.

Osteoblasts were visible on the surface of the bone trabeculae, and typical osteocytes were found in the bone lacunae.

In the scientific literature, we have also found works on the study of similar biomaterials for the healing of long bone defects. For example, Bhattacharjee P. and co-authors, using the histological method and scanning electron microscopy, found that hydroxyapatite loaded with zinc on the 60th day after implantation into the defect of the medial part of the proximal tibial diaphysis (5 mm × 2. 5 mm × 3 mm) of New Zealand rabbits demonstrated direct and dense contact with the formed lamellar bone tissue of the regenerate and better osseointegration compared to hydroxyapatite, unloaded with zinc [8]. Olmez S. S. and co-authors histologically found during 60 days of observation in New Zealand rabbits that chitosan/alginate gels and sponges in a 1 cm radius defect were initially surrounded by a thin layer of connective tissue, and later there was a reorganization of fibrous tissue and integration of implants into bone tissue formed by the intramembranous pathway [32].

In our experiment, on day 90, connective tissue was still detected in the control group animals and in the area of S2/DCPD implantation. However, the area of the previous injury was filled mainly with regenerated bone tissue with S2/DCPD fragments integrated into its structures. However, in animals of the second group, connective tissue was not detected in the area of injury at all, and the majority of the defect area was occupied by the S1/HA-Zn biomaterial, without visible signs of fragmentation and resorption. At the same time, S1/HA-Zn was fully integrated into the bone tissue of the regenerate, which had a lamellar structure, with osteocytes with long processes in the lacunae. In addition, in our opinion, a significant difference between the two materials was that osteogenic cellular elements formed new bone tissue not only on the outer surface of S1/HA-Zn but also in the middle of this scaffold, whereas we did not observe osteogenic cells and foci of osteogenesis in the middle of S2/DCPD.

In turn, Kresakova L. and co-authors 6 months after implantation of HA of various geometric shapes (cylinder, plates with holes and without holes) into the defect (diameter of about 6 mm and about 15 mm deep) of the distal end of the metatarsal bone of a sheep of the wolf/merino breed found that all implants demonstrated excellent biocompatibility, no connective tissue was identified at the border between the biomaterial and the regenerate bone tissue, and the scaffolds were in close contact with the bone tissue, demonstrating good osseointegration and osteoconductive properties. It should also be noted that closer to the central parts of the biomaterials in the form of a cylinder, bone islands were identified, hydroxyapatite plates with holes were resorbed, and hydroxyapatite plates without holes were not resorbed [33].

In our study, at the last follow-up period (140 days), S2/DCPD and S1/HA-Zn implants were integrated only into the regenerated bone tissue, which had a typical lamellar structure. It contained osteocytes and sometimes single multinucleated osteoclasts. At the same time, new bone tissue with osteons was formed not only on the outer surface of S1/HA-Zn. Small foci of osteogenesis were also observed in the middle of the S1/HA-Zn scaffold. This phenomenon was the main difference between the S1/HA-Zn biomaterial and S2/DCPD since no foci of osteogenesis were observed in the middle of S2/DCPD at all stages of the experiment. No complete resorption of any biomaterial occurred during the 140-day experiment, and in general, the biodegradation of all the studied scaffolds was slow. This is especially true for S1/HA-Zn, which did not change its size or geometric shape during 140 days in the defect and occupied a significant area of the previous injury.

5. Conclusions

The influence of two nanostructured osteoplastic materials with different compositions: i) alginate (Alg) matrix, loaded with Zn^{2+} ions and nanostructured HA - S1/HA/Zn, and ii) CS matrix loaded with DCPD NPs - S2/DCPD on the healing of an experimental femoral diaphysis defect was investigated. The natural polymers alginate (anionic) and chitosan (cationic) have opposite electrostatic natures, which affects the properties of composites based on them. Microscopic examination showed that no signs of an inflammatory reaction were observed in the implantation site of S2/DCPD and S1/HA-Zn during the entire experiment. Both biomaterials have a positive effect on the dynamics of bone wound healing, but the regenerative potential of S1/HA-Zn is significantly higher than that of S2/DCPD. It is noteworthy that the formation of new bone tissue occurred both on the surface of the S1/HA-Zn bead and in its interior. S2/DCPD first integrates into the connective tissue, then into the bone tissue that forms on the outer composite's surface. The study demonstrated the EM structure of cellular elements and the lacunar tubular system of regenerated bone tissue. The regenerated bone tissue contained osteocytes located in bone lacunae, and osteoblasts were located on the surface of bone trabeculae. Single multinucleated osteoclasts were observed in the bone tissue, which formed resorption lacunae.

Ethics statement

All experiments involving laboratory animals were conducted in accordance with the EU Directive 2010/63/EU for animal experiments after approval by the Commission for Bioethics in Experimental and Clinical Research of Sumy State University (Protocol No. 1/6 of 30.06.2023).

Data availability statement

Data will be made available on request.

Funding

The research was financially supported by the National Research Foundation of Ukraine within the framework of the program Science for Security and Sustainable Development of Ukraine 0122U001154.

CRediT authorship contribution statement

Oleksii Korenkov: Writing – review & editing, Writing – original draft, Visualization, Methodology, Investigation, Data curation. **Liudmyla Sukhodub:** Writing – review & editing, Writing – original draft, Formal analysis, Conceptualization. **Mariia Kumeda:** Visualization. **Olha Sukhonos:** Investigation. **Leonid Sukhodub:** Writing – review & editing, Supervision, Resources, Project administration, Funding acquisition.

Declaration of competing interest

The authors declare that they have no known competing financial interests or personal relationships that could have appeared to influence the work reported in this paper.

References

[1] S.S. Lee, X. Du, I. Kim, S.J. Ferguson, Scaffolds for bone-tissue engineering, Materials 5 (9) (2022) 2722–2759, https://doi.org/10.1016/j.matt.2022.06.003.
[2] Z. Morsada, et al., Recent progress in biodegradable and bioresorbable materials: from passive implants to active electronics, Appl. Mater. Today 25 (2021) 101257.
[3] T. Fischetti, et al., 3d printing and bioprinting to model bone cancer: the role of materials and nanoscale cues in directing cell behavior, Cancers 13 (2021) 16.
[4] H. Yukawa, K. Sato, Y. Baba, Theranostics applications of quantum dots in regenerative medicine, cancer medicine, and infectious diseases, Adv. Drug Deliv. Rev. 200 (2023 Sep) 114863, https://doi.org/10.1016/j.addr.2023.114863.
[5] Y. Huang, L. Wang, Experimental studies on nanomaterials for soil improvement: a review, Environ. Earth Sci. 75 (2016) 6.
[6] J.P. Monte, A. Fontes, B.S. Santos, G.A.L. Pereira, G. Pereira, Recent advances in hydroxyapatite/polymer/silver nanoparticles scaffolds with antimicrobial activity for bone regeneration, Mater. Lett. 338 (2023) 134027, https://doi.org/10.1016/j.matlet.2023.134027.
[7] V.A. Bhardwaj, P.C. Deepika, S. Basavarajaiah, Zinc incorporated nano hydroxyapatite: a novel bone graft used for regeneration of intrabony defects, Contemp. Clin. Dent. 9 (3) (2018) 427–433, https://doi.org/10.4103/ccd.ccd_192_18.
[8] P. Bhattacharjee, H. Begam, A. Chanda, S.K. Nandi, Animal trial on zinc doped hydroxyapatite: a case study, Journal of Asian Ceramic Societies 2 (1) (2014) 44–51, https://doi.org/10.1016/j.jascer.2014.01.005.
[9] Z. He, C. Jiao, J. Wu, J. Gu, H. Liang, L. Shen, Y. Yang, Z. Tian, C. Wang, Q. Jiang, Zn-doped chitosan/alginate multilayer coatings on porous hydroxyapatite scaffold with osteogenic and antibacterial properties, Int J Bioprint 9 (2) (2023) 668, https://doi.org/10.18063/ijb.v9i2.668.
[10] E.S. Thian, T. Konishi, Y. Kawanobe, P.N. Lim, C. Choong, B. Ho, M. Aizawa, Zinc-substituted hydroxyapatite: a biomaterial with enhanced bioactivity and antibacterial properties, J. Mater. Sci. Mater. Med. 24 (2) (2013) 437–445, https://doi.org/10.1007/s10856-012-4817-x.
[11] M.H. Fernandes, M.M. Alves, M. Cebotarenco, I.A.C. Ribeiro, L. Grenho, P.S. Gomes, M.J. Carmezim, C.F. Santos, Citrate zinc hydroxyapatite nanorods with enhanced cytocompatibility and osteogenesis for bone regeneration, Mater. Sci. Eng., C 115 (2020) 111147, https://doi.org/10.1016/j.msec.2020.111147.
[12] X. Fu, Y. Li, T. Huang, Z. Yu, K. Ma, M. Yang, Q. Liu, H. Pan, H. Wang, J. Wang, M. Guan, Runx2/Osterix and zinc uptake synergize to orchestrate osteogenic differentiation and citrate containing bone apatite formation, Adv Sci (Weinh) 5 (4) (2018) 1700755, https://doi.org/10.1002/advs.201700755.
[13] M. Molenda, J. Kolmas, The role of zinc in bone tissue health and regeneration-a review, Biol. Trace Elem. Res. 201 (12) (2023) 5640–5651, https://doi.org/10.1007/s12011-023-03631-1.
[14] S. Dhivya, S. Saravanan, T. Sastry, N. Selvamurugan, Nanohydroxyapatitereinforced chitosan composite hydrogel for bone tissue repair in vitro and in vivo, J. Nanobiotechnol. 13 (2015), https://doi.org/10.1186/s12951-015-0099-z.
[15] A. Pogrebnjak, L. Sukhodub, L. Sukhodub, O. Bondar, M. Kumeda, B. Shaimardanova, A. Turlybekuly, Composite material with nanoscale architecture based on bioapatite, sodium alginate and ZnO microparticles, Ceram. Int. 45 (6) (2019) 7504–7514, https://doi.org/10.1016/J.CERAMINT.2019.01.043.
[16] R.C. Cuozzo, M.H.M.R. Leão, L.A. Gobbo, D.N. Rocha, N.M.E. Ayad, W. Trindade, A.M. Costa, M.H.P. Silva, Zinc alginate–hydroxyapatite composite microspheres for bone repair, Ceram. Int. 40 (7) (2014) 11369–11375, https://doi.org/10.1016/j.ceramint.2014.02.107.
[17] A. Issabayev, T. Fazylov, M. Temirbayev, M. Kopbayeva, N. Duisenov, M. Kamyspaev, S. Tanabayeva, I. Fakhradiyev, The Impact of Nano-Crystal Hydroxyapatites on the Regeneration of Bone Defects, Experimental and Applied Biomedical Research (EABR), 2021, https://doi.org/10.2478/sjecr-2021-0053.
[18] G. Tang, Z. Liu, Y. Liu, J. Yu, X. Wang, Z. Tan, X. Ye, Recent trends in the development of bone regenerative biomaterials, Front. Cell Dev. Biol. 9 (2021) 665813, https://doi.org/10.3389/fcell.2021.665813.
[19] B. Zwingenberger, C. Vater, R.L. Bell, J. Bolte, E. Mehnert, R. Brünler, D. Aibibu, S. Zwingenberger, Treatment of critical-size femoral bone defects with chitosan scaffolds produced by a novel process from textile engineering, Biomedicines 9 (8) (2021) 1015, https://doi.org/10.3390/biomedicines9081015.
[20] A. Safira, C.A.M. Rani, F. Fikri, A. Purnomo, S. Khairani, S. Chhetri, S.T. Maslamama, M.T.E. Purnama, Hydroxyapatite-chitosan composites derived from sea cucumbers and shrimp shells ameliorate femoral bone defects in an albino rat model, Vet. World 16 (5) (2023 May) 1084–1091, https://doi.org/10.14202/vetworld.2023.1084-1091.
[21] N. Ramesh, S.C. Moratti, G.J. Dias, Hydroxyapatite-polymer biocomposites for bone regeneration: a review of current trends, J. Biomed. Mater. Res. B Appl. Biomater. 106 (5) (2018) 2046–2057, https://doi.org/10.1002/jbm.b.33950.
[22] Z. Li, H.R. Ramay, K.D. Hauch, D. Xiao, M. Zhang, Chitosan-alginate hybrid scaffolds for bone tissue engineering, Biomaterials 26 (18) (2005) 3919–3928, https://doi.org/10.1016/j.biomaterials.2004.09.062.
[23] M. Sattary, M. Rafienia, M. Kazemi, H. Salehi, M. Mahmoudzadeh, Promoting effect of nano hydroxyapatite and vitamin D3 on the osteogenic differentiation of human adipose-derived stem cells in polycaprolactone/gelatin scaffold for bone tissue engineering, Mater. Sci. Eng. C 97 (2019) 141–155, https://doi.org/10.1016/j.msec.2018.12.030.
[24] H. Kato, H. Ochiai-Shino, S. Onodera, A. Saito, T. Shibahara, T. Azuma, Promoting effect of 1,25(OH)2 vitamin D3 in osteogenic differentiation from induced pluripotent stem cells to osteocyte-like cells, Open Biol 5 (2) (2015) 140–201, https://doi.org/10.1098/rsob.140201.
[25] A. Pogrebnjak, L. Sukhodub, L. Sukhodub, O. Bondar, M. Kumeda, B. Shaimardanova, et al., Composite material with nanoscale architecture based on bioapatite, sodium alginate and ZnO microparticles, Ceram. Int. (2019), https://doi.org/10.1016/j.ceramint.2019.01.043.
[26] L. Sukhodub, M. Kumeda, L. Sukhodub, V. Strelchuk, I. Nasieka, L. Vovchenko, et al., Hybrid composite based on chitosan matrix mineralized by polyphasic calcium orthophosphates with enhanced bioactivity and protein adsorption capacity, Mater. Today Commun. 31 (2022), https://doi.org/10.1016/j.mtcomm.2022.103696.
[27] L.B. Sukhodub, M. Kumeda, V. Bielai, L.F. Sukhodub, Hydroxyapatite-biopolymers-ZnO composite with sustained Ceftriaxone release as a drainage system for treatment of purulent cavities, Carbohydr. Polym. 266 (2021) 118137, https://doi.org/10.1016/j.carbpol.2021.118137.
[28] L.F. Sukhodub, L.B. Sukhodub, O. Litsis, Y. Prylutskyy, Synthesis and characterization of hydroxyapatite-alginate nanostructured composites for the controlled drug release, Mater. Chem. Phys. 217 (2018) 228–234, https://doi.org/10.1016/j.matchemphys.2018.06.071.
[29] L. Sukhodub, M. Kumeda, L. Sukhodub, L. Vovchenko, V. Prokopiuk, O. Petrenko, I. Kovalenko, R. Pshenychnyi, A. Opanasyuk, Effect of zinc oxide micro- and nanoparticles on cytotoxicity, antimicrobial activity and mechanical properties of apatite-polymer osteoplastic material, J. Mech. Behav. Biomed. Mater. 150 (2024) 106289, https://doi.org/10.1016/j.jmbbm.2023.106289.
[30] F.A. Shah, K. Ruscsák, A. Palmquist, 50 years of scanning electron microscopy of bone – a comprehensive overview of the important discoveries made and insights gained into bone material properties in health, disease and taphonomy, Bone Res 7 (1) (2019) 1–15, https://doi.org/10.1038/s41413-019-0053-z.

[31] Olexii Korenkov, Liudmyla Sukhodub, Mariia Kumeda, Leonid Sukhodub, In Vivo feature of the regenerative potential of chitosan and alginate based osteoplastic composites doped with calcium phosphates, zinc ions, and vitamin D2, Ann. Anat. (2024) 152290, https://doi.org/10.1016/j.aanat.2024.152290.
[32] S.S. Olmez, P. Korkusuz, H. Bilgili, S. Senel, Chitosan and alginate scaffolds for bone tissue regeneration, Pharmazie 62 (6) (2007) 423–431, https://doi.org/10.1691/ph.2007.6.6140.
[33] L. Kresakova, L. Medvecky, K. Vdoviakova, M. Varga, J. Danko, R. Totkovic, T. Spakovska, M. Vrzgula, M. Giretova, J. Briancin, V. Šimaiová, M. Kadasi, Long-bone-regeneration process in a sheep animal model, using hydroxyapatite ceramics prepared by tape-casting method, Bioengineering (Basel) 10 (3) (2023) 291, https://doi.org/10.3390/bioengineering10030291.